Local energy transfer rate and kinetic processes: the fate of turbulent energy in two-dimensional Hybrid Vlasov-Maxwell numerical simulations

Journal:	*Journal of Plasma Physics*
Manuscript ID	PLA-2018-0031.R1
Special Collection:	Special Collection in Honor of the 70th Birthday of Professor Francesco Pegoraro
Date Submitted by the Author:	n/a
Complete List of Authors:	Sorriso-Valvo, Luca; CNR, Nanotec Perrone, Denise; Imperial College of London, Department of Physics; European Space Astronomy Centre, ESAC Pezzi, Oreste; University of Calabria, Physics Valentini, Francesco; University of Calabria, Physics Servidio, Sergio; Universita degli Studi della Calabria, Dipartimento di Fisica Zouganelis, Yoannis; European Space Astronomy Centre, ESAC Veltri, Pierluigi; University of Calabria, Department of Physics
Keywords:	Plasma Nonlinear Phenomena, Plasma Simulation, Space Plasma Physics

SCHOLARONE™
Manuscripts

Local energy transfer rate and kinetic processes: the fate of turbulent energy in two-dimensional Hybrid Vlasov-Maxwell numerical simulations

Luca Sorriso-Valvo[1]†, Denise Perrone[2,3], Oreste Pezzi[4], Francesco Valentini[4], Sergio Servidio[4], Ioannis Zouganelis[2] & Pierluigi Veltri[4]

[1]Nanotec/CNR, Sede di Cosenza, Ponte P. Bucci, Cubo 31C, 87036 Rende, Italy.
[2]European Space Agency, ESAC, Madrid, Spain.
[3]Department of Physics, Imperial College London, London SW7 2AZ, United Kingdom.
[4]Dipartimento di Fisica, Università della Calabria, Ponte P. Bucci, Cubo 31C, 87036 Rende, Italy.

(Received ?; revised ?; accepted ?. - To be entered by editorial office)

The nature of the cross-scale connections between the inertial range turbulent energy cascade and the small-scale kinetic processes in collisionless plasmas is explored through the analysis of two-dimensional Hybrid Vlasov-Maxwell numerical simulation (HVM), with α particles, and through a proxy of the turbulent energy transfer rate, namely the Local Energy Transfer rate (LET). Correlations between pairs of variables, including those related to kinetic processes and to deviation from Maxwellian distributions, are first evidenced. Then, the general properties and the statistical scaling laws of the LET are described, confirming its reliability for the description of the turbulent cascade and revealing its textured topology. Finally, the connection between such proxy and the diagnostic variables is explored using conditional averaging, showing that several quantities are enhanced in the presence of large positive energy flux, and reduced near sites of negative flux. These observations can help determining which processes are involved in the dissipation of energy at small scales, as for example ion-cyclotron or mirror instabilities typically associated with perpendicular anisotropy of temperature.

PACS codes: Authors should not enter PACS codes directly on the manuscript, as these must be chosen during the online submission process and will then be added during the typesetting process (see http://www.aip.org/pacs/ for the full list of PACS codes)

For Review

1. Introduction

The dynamical behavior of plasmas depends markedly on frequencies and scales. At low frequencies and large scales, ions and electrons are locked together and behave like an electrically conducting fluid; this is the regime of magnetohydrodynamics (MHD). At higher frequencies and smaller scales, electrons and ions can move relative to each other, behaving like two separate and interpenetrating fluids: this is the two-fluid regime. However, if the dynamics is supported by non-thermal effects and anisotropies in the velocity space, the more complete kinetic theory shall be adopted. A notable example is represented by the solar wind, a continuous, highly variable, weakly collisional plasma

† Email address for correspondence: lucasorriso@gmail.com

outflowing at high speed from the Sun. This complex medium is highly structured, with turbulent fluctuations on a wide range of scales, from fractions of a second to several hours, thus covering all the above dynamical ranges.

Spacecraft measurements have revealed that the solar-wind plasma is usually in a state of fully developed turbulence (Marsch 2006; Bruno & Carbone 2013; Alexandrova *et al.* 2013). As the turbulent fluctuations expand away from the Sun, these decay and transfer energy to smaller scales. At scales comparable with the ion gyro-radius or the ion inertial length, the MHD approximation fails and kinetic processes involving field-particle interactions take place, along with important cross-scale coupling (Schwartz *et al.* 2011). Furthermore, since the plasma collisionality is quite low, the ion and electron velocity distribution functions can exhibit significant non-Maxwellian signatures. Kinetic processes manifest through the excitation of plasma waves, temperature anisotropy, plasma heating, particle energization, entropy cascade, excitation of plasma waves and so on (Vaivads *et al.* 2016). Recently, a phenomenological description in terms of cascade in the velocity space, due to highly structured particle distributions, has been proposed (Schekochihin *et al.* 2016; Servidio *et al.* 2017). Observations based on the high-resolution ion velocity distribution measurements by the Magnetospheric Multiscale (MMS) mission in the Earth's turbulent magnetosheath (Servidio *et al.* 2017) have recently confirmed such description, opening a new pathways to the understanding of plasma turbulence and dissipation in collisionless plasmas. **Numerical simulations are even investigating these features (Pezzi et al. 2018; Cerri *et al.* 2018)**. This cascade may efficiently transfer the energy towards smaller velocity scales, thus producing finer structures in the particle velocity distribution function. The presence of such structures may ultimately enable and enhance the effect of collisions in dissipating the energy (Pezzi *et al.* 2013, 2014, 2015a,b, 2016; Pezzi 2017). Numerical simulations represent an indispensable tool for the understanding of plasma nonlinear dynamics. The use of kinetic numerical simulations is crucial, indeed, when kinetic processes occur in turbulent collisionless plasmas (Parashar *et al.* 2009; Camporeale & Burgess 2011; Servidio *et al.* 2015; Franci *et al.* 2015; Cerri *et al.* 2016, 2017; Groselj *et al.* 2017; Franci *et al.* 2018). The Eulerian hybrid Vlasov-Maxwell *HVM* code (Valentini *et al.* 2007; Perrone *et al.* 2011) can be used to study the dynamics of a turbulent plasma with typical solar wind conditions, in order to describe the cross-scale coupling between the MHD turbulence and the small-scale kinetic processes (Valentini *et al.* 2008; Valentini & Veltri 2009; Valentini *et al.* 2010, 2011a,b; Perrone *et al.* 2011; Servidio *et al.* 2012; Greco *et al.* 2012; Perrone *et al.* 2013; Servidio *et al.* 2014; Perrone *et al.* 2014a,b; Valentini *et al.* 2014; Servidio *et al.* 2015; Valentini *et al.* 2016; Pezzi *et al.* 2017a,b).

For numerical simulations of kinetic turbulence that also include an extended fluid range, the energy level of the small-scale fluctuations may be too low to be investigated with Lagrangian algorithms, unless a large number of particles per cell is used (Franci *et al.* 2015). For a convergence study in PIC codes see Haggerty *et al.* (2017). Eulerian-based numerical algorithms might be more suitable for this scope. HVM simulations show that kinetic effects produce, close to reconnection regions, a distortion of the ion velocity distribution, through the generation of accelerated field-aligned beams, temperature anisotropy and trapped particle populations. Moreover, **although the addition of heavy ions does not considerably affect the inertial-range turbulent cascade (Perrone *et al.* 2013),** departures from the Maxwellian shape are more pronounced for heavy ions than for protons (Perrone *et al.* 2013, 2014b; Valentini *et al.* 2016), pointing out that the role of secondary ions must be considered for understanding energy partition in plasmas (Marsch 2006; Kasper *et al.* 2008; Araneda *et al.* 2009; Maneva *et al.* 2015). Although the physical mechanisms

For Review Only

of solar wind turbulence have been matter of investigation for many decades, both using 'in situ' measurements and numerical experiments, important problems concerning the interconnection between the inertial and kinetic range processes, as well as the interplay between physical space fluctuations and velocity space perturbations, are still poorly understood.

Solar wind turbulence is characterized by intermittency (Burlaga 1991; Frisch 1995), *i.e.* the spatial inhomogeneity of the energy transfer across scales, that results in the generation of highly energetic, bursty small-scale fluctuations with scale-dependent, non-Gaussian statistics (Sorriso-Valvo *et al.* 1999). Such fluctuations are often referred to as coherent structures, with phase synchronization among a certain number of scales (Greco & Perri 2014; Lion *et al.* 2016; Roberts *et al.* 2016; Perrone *et al.* 2016, 2017). At smaller scales, below the MHD range, a more variable level of intermittency is observed, whose nature is still under debate (Alexandrova *et al.* 2008; Kiyani *et al.* 2009). During latest years, the study of the intermittency and the consequent research on small-scale structures have been performed by using different methods. For example, wavelet analysis (Farge 1992; Bruno *et al.* 1999) provides the local estimation of the scale-dependent energy associated with the magnetic fluctuations, thus allowing the identification of the highly energetic intermittent structures. Alternatively, the Partial Variance of Increments (PVI) technique (Greco *et al.* 2008) was used to identify discontinuities, current sheets, and other intermittent features.

Recently, there is a compelling evidence that the kinetic processes are enhanced in the proximity of the turbulence-generated structures, which carry a larger amount of energy than the turbulent background. Measurements have shown that both ions and electrons are energized in the proximity of the most intense small-scale current sheets (Osman *et al.* 2011, 2012; Tessein *et al.* 2013; Chasapis *et al.* 2015, 2017). Note that the same behavior has been observed in HVM numerical simulations (Servidio *et al.* 2012; Greco *et al.* 2012; Perrone *et al.* 2014b). More recently, even reduced models such as gyro-kinetics converged toward this general view (Howes 2016; Howes *et al.* 2018). The processes responsible for such different forms of energization may involve magnetic reconnection (Retinò *et al.* 2007; Burch *et al.* 2016b), wave-particle resonances, plasma instabilities (Matteini *et al.* 2013; Servidio *et al.* 2014; Breuillard *et al.* 2016) and enhancement of collisions (Pezzi *et al.* 2016). These topics are currently very debated in the space plasma community (Chen 2016).

In order to understand the interconnections between the turbulent structures and the small-scale kinetic processes, a more detailed description of the local energy flux across scales should be defined for plasma turbulence. This possible tool should take into account the complex nature of the nonlinear coupling between velocity and magnetic field. Recent studies included the contributions from cross-terms, typically associated to Alfvénic fluctuations, to better identify regions of small-scale accumulation of energy (Sorriso-Valvo *et al.* 2015).

In MHD, the energy transfer across scales obeys the Politano-Pouquet law (PP) (Politano & Pouquet 1998), which prescribes the linear scaling of the mixed third-order moment of the fields increments. The proportionality factor is the mean energy transfer rate $\langle \epsilon^{\pm} \rangle$, the brackets indicating ensemble average. For a two-dimensional field, the standard version of the PP law for the the mixed third-order moments $Y^{\pm}(l)$ is

$$Y^{\pm}(l) = \langle |\Delta \mathbf{z}^{\pm}{}_{l}(\mathbf{r})|^2 \, \Delta z^{\mp}_{i,l}(\mathbf{r}) \rangle = -2 \langle \epsilon^{\pm} \rangle l \; . \tag{1.1}$$

$\Delta \psi_l = \psi(\mathbf{r} + l\mathbf{r}/r) - \psi(\mathbf{r})$ is the longitudinal increment of a generic field ψ (e.g. the magnetic field $\mathbf{B}(\mathbf{r})$) across the scale l; the subscript i indicates the generic component of the field, the field increment being estimated along the same direction; $\mathbf{z}^{\pm} = \mathbf{v} \pm \mathbf{B}/\sqrt{4\pi\rho}$

For Peer Review

are the Elsasser variables that couple the plasma velocity $\mathbf{v}$ and the magnetic field $\mathbf{B}$, the latter being expressed in velocity units through the plasma density ρ. The validity of the PP law has been first verified in two-dimensional MHD numerical simulations (Sorriso-Valvo *et al.* 2002), and later also in the solar wind (MacBride *et al.* 2005; Sorriso-Valvo *et al.* 2007; Marino *et al.* 2008; MacBride *et al.* 2008; Marino *et al.* 2012).

Based on the PP law (Equation 1.1), an heuristic proxy of the 'local' energy transfer rate (LET) at the scale l can be defined by introducing the quantity:

$$\epsilon_l(\mathbf{r}) = -\frac{1}{2l}\left[|\Delta\mathbf{z}^+{}_l(\mathbf{r})|^2\,\Delta z^-_{i,l}(\mathbf{r}) + |\Delta\mathbf{z}^-{}_l(\mathbf{r})|^2\,\Delta z^+_{i,l}(\mathbf{r})\right]\,. \tag{1.2}$$

At a given scale, each field increment in the time series can thus be associated with the local value of $\epsilon_l(\mathbf{r})$ (Marsch & Tu 1997; Sorriso-Valvo *et al.* 2015, 2018). Note that the LET can be expressed in terms of velocity and magnetic field as $\epsilon_l(\mathbf{r}) \propto \Delta v_i(\Delta v^2 + \Delta b^2) - 2\Delta b_i(\Delta\mathbf{v}\cdot\Delta\mathbf{b})$. The first right-hand-side term is associated with the total energy advected by the velocity fluctuations, **and is correlated to the total PVI (*i.e.* including both velocity and magnetic increments)**. The second term is associated with the velocity-magnetic field correlations coupled to the longitudinal magnetic field fluctuations (Andrés & Sahraoui 2017; Sorriso-Valvo *et al.* 2018). Recently, by using Helios 2 data, it has been shown that the LET correctly identifies the regions of space in the turbulent solar wind that carry energy towards smaller scales. These regions are characterized by enhanced kinetic processes, resulting in higher proton temperature (Sorriso-Valvo *et al.* 2018). It is worth noting that in recent works, the third order law in Eq. (1.1) has been extended to include characteristic plasma length scales and compressibility (Andrés *et al.* 2018).

The correlation between the local temperature increase and the large amplitude bursts of energy transfer suggests that the proxy defined in Eq. (1.2) might play an important role in the understanding of solar wind turbulent dissipation and heating. Moreover, the comparison between the properties of the PVI and LET has shown that both methods are suitable for the description of the turbulent energy cascade, **although the LET carries additional information related to the correlations between velocity magnetic turbulent fluctuations. Additionally**, since the LET is a signed variable, in principle it should also carry additional information about the possible direction of the cross-scale energy flow, identifying possible local direct and inverse cascade processes. The latter cannot be studied by using PVI or wavelet-based techniques since these are positive-defined.

The aim of this paper is to explore the link between the MHD turbulent energy cascade and the kinetic processes associated with deviations of the ion velocity distributions from the Maxwellian equilibrium. To this aim, we make use of the LET for interpreting high-resolution data from numerical simulations of the Vlasov-Maxwell multi-component system. The present work is organized as follows. In Section 2 the governing equations, the numerical algorithm and the parameters of the Vlasov simulations will be presented. A brief overview on the numerical results will be given. The use of the proxy of the local energy transfer rate will be the topic of Section 3, while in Section 4 we will discuss our conclusions.

2. HVM multi-component simulations

We use high resolution Vlasov simulations in order to simulate the turbulent multi-species plasma of the solar wind. First, high spatial resolution is needed in order to follow the evolution of the turbulent cascade up to wavelengths shorter than ion characteristic scales, where kinetic effects presumably govern the physics of the system. Second, high

For Peer Review

numerical resolution in the velocity domain is required to investigate the distortions of the ion distribution functions. The above two requirements are the main ingredients of the highly-performing, extensively tested, HVM code (http://fis.unical.it/hvm/).

2.1. *Numerical method*

We employ the HVM code which directly integrates the Vlasov equations for both proton and α particle distribution functions while electrons are considered as a massless isothermal fluid. The Vlasov equation for both ion species is combined with the Maxwell system, by assuming quasi-neutrality and by neglecting the displacement current. In particular Ampére and Faraday equations and a generalized Ohm's law are solved. HVM equations, written in dimensionless form, are the following:

$$\frac{\partial f_s}{\partial t} + \mathbf{v} \cdot \frac{\partial f_s}{\partial \mathbf{r}} + \lambda_s \left(\mathbf{E} + \mathbf{v} \times \mathbf{B}\right) \cdot \frac{\partial f_s}{\partial \mathbf{v}} = 0 \tag{2.1}$$

$$\mathbf{E} = -\left(\mathbf{u}_e \times \mathbf{B}\right) - \frac{\nabla P_e}{n_e} + \eta \mathbf{j} \tag{2.2}$$

$$\frac{\partial \mathbf{B}}{\partial t} = -\nabla \times \mathbf{E} \quad ; \quad \nabla \times \mathbf{B} = \mathbf{j} \tag{2.3}$$

In previous equations, $f_s(\mathbf{r}, \mathbf{v}, t)$ is the ion distribution function (the subscript $s = p, \alpha$ refers to protons and α particles, respectively), $\mathbf{E}(\mathbf{r}, t)$ and $\mathbf{B}(\mathbf{r}, t)$ are the electric and magnetic fields, respectively, and λ_s is a constant reflecting the charge to mass ratio of each species ($\lambda_p = 1$, $\lambda_\alpha = 1/2$). The electron bulk speed is $\mathbf{u}_e = \left(\sum_s Z_s n_s \mathbf{u}_s - \mathbf{j}\right)/n_e$, where Z_s is the ion charge number ($Z_p = 1$, $Z_\alpha = 2$), the ion density n_s and the ion bulk velocity $\mathbf{u}_s$ are the zero-th and first order moments of the ion distribution function, respectively, and the electron density n_e is evaluated through the quasi-neutrality condition $n_e = \sum_s Z_s n_s$. Furthermore, $P_e = n_e T_e$ is the electron pressure (T_e is homogeneous and stationary) and $\mathbf{j} = \nabla \times \mathbf{B}$ is the total current density. The external small resistivity $\eta = 2 \times 10^{-2}$ is introduced to remove spurious numerical instabilities. In Equations (2.1)–(2.3), masses, charges, time, velocities and lengths are respectively normalized to the proton mass, m_p, and charge, e, to the inverse of the proton cyclotron frequency, $\Omega_{cp}^{-1} = m_p c / e B_0$ (being c and B_0 the speed of light and the ambient magnetic field), to the Alfvén velocity, $V_A = B_0/\sqrt{4\pi n_{0,p} m_p}$ (being $n_{0,p}$ the equilibrium proton density), and to the proton skin depth, $d_p = V_A/\Omega_{cp}$.

The described set of Equations (2.1)–(2.3) are solved in a $2.5D - 3V$ phase space domain, where $2.5D$ means that all vector components are retained but they depend only on the two spatial coordinates (x, y). The spatial domain, whose size is $L = 2\pi \times 20 d_p$ in both directions, has been discretized with 512^2 grid-points and, at boundaries, periodic conditions are implemented. Each direction of the velocity domain of each species (protons and α particles) is discretized with 71 grid-points in the range $v_{j,s} = [-v_{max,s}, v_{max,s}]$ $(j = x, y, z)$, where $v_{max,s} = \pm 5 v_{th,s}$ (being $v_{th,s} = \sqrt{k_B T_{0,s}/m_s}$ the ion thermal speed, with $T_{0,s}$ the equilibrium temperature). Boundary conditions in velocity space assume $f_s(|v| > v_{max,s}) = 0$ in each direction. The time step Δt has been chosen in such a way that the CFL condition for the numerical stability of the Vlasov algorithm is satisfied (Peyret & Taylor 1986). To control the numerical accuracy of the simulation, the basic set of conservation laws of Vlasov equation is continuously monitored during the simulations: relative variation of proton mass, α particle mass, total energy and entropy are about $2.5 \times 10^{-3}\%$, $3.5 \times 10^{-1}\%$, 0.6% and 0.4%, respectively.

At the initial time of the simulation ($t = 0$), both ion species have Maxwellian distribution functions, with homogeneous densities, and an uniform background out-of-plane magnetic field $\mathbf{B_0} = B_0 \mathbf{e}_z$ is imposed. In order to mimic the physical conditions

For Review Only

of the pristine solar wind, we assume that i) the α particle to proton density ratio $n_{0,\alpha}/n_{0,p} = 5\%$ and ii) we consider α particles, protons and electrons at the same initial temperature $T_{0,\alpha} = T_{0,p} = T_e$. The equilibrium is then perturbed through a $2D$ spectrum of Fourier modes in the plane (x, y), for both proton bulk velocity and magnetic field, such that proton bulk velocity and magnetic field are globally uncorrelated. Energy is injected with wave numbers in the range $0.1 < k < 0.3$ ($2 \leq m \leq 6$, where $k = 2\pi m/L$) and random phases. We did not introduce neither density disturbances nor parallel variances, i.e. $\delta n = \delta u_z = \delta B_z = 0$ at $t = 0$. The r.m.s. level of fluctuations is $\delta B/B_0 = 1/3$, while $\beta_p = 2v_{th,p}^2/V_A^2 = 0.5$.

The kinetic evolution of protons and α particles is numerically investigated in a decaying turbulence. During the simulation, nonlinear couplings between fluctuations generate a turbulent cascade, where the injected energy is transferred along the spectrum to smaller, kinetic scales. The time t^* of maximum turbulent activity can be identified as the peak time of the spatially averaged out-of-plane current density, $\langle j_z^2 \rangle$, a standard indicator for small-scale magnetic gradients. All the analysis has been performed using one snapshot of the simulation at $t^*\Omega_{cp} = 49$, when decaying turbulence approaches a quasi-steady state. A more detailed description of the numerical results of the simulation can be found in Valentini *et al.* (2016).

2.2. *Numerical results*

An overview of the differential kinetic dynamics of the ion species, namely protons and α particles, associated to the development of the turbulent cascade, is presented in Figure 1. Turbulence leads to the generation of small-scale coherent structures, such as current sheets, filaments, or strongly shared flows, which can be recognized in the two-dimensional patterns in physical space. In particular, panel (a) of Figure 1 shows the shaded contours of the out-of-plane current density, j_z. The current density becomes very intense in between magnetic islands, where magnetic reconnection can locally occur.

Panel (b) shows the contour map of the local energy transfer rate, $\epsilon_l(x, y)$, estimated using the velocity and magnetic field (in Alfvén units) two-point increments at the scale $l = d_p$. Positive and negative filaments of strong energy transfer ϵ_l are present, but the spatial correlation with strong current sheets is unclear. There is a shift between the current layers and this cascade-transfer indicator, probably due to the fact that the former are the sites of dissipation, while the LET is high at the very active nonlinear regions, such as the upstream parts of the reconnecting current sheets.

In panel (c) we display the contour map of $\mathbf{E} \cdot \mathbf{j}$, a proxy of energy conversion between fields and particles (Wan *et al.* 2015; Yang *et al.* 2017). Large positive values are observed in the proximity of the strongest current sheets, suggesting that the electromagnetic energy might be converted into kinetic and thermal energy where magnetic reconnection is likely to occur.

Panels (d) and (g) of Figure 1 show the maps of proton and α-particle temperature, respectively, **defined as the second-order velocity moment of the ion distribution function**. Comparison with panel (a) highlights that the presence of strong current sheets corresponds to temperature enhancement of both ions. Although the initial conditions of the simulation infer equal and uniform temperature for the two ion species, during the turbulent evolution of the system both ions show a non-uniform temperature pattern, with similar inhomogeneity as for the current j_z. Color bars were chosen so that the initial temperature T_0 is white, while red and blue indicate local heating and cooling, respectively. A definite temperature increase can be observed close to the region of strong magnetic field gradients, meaning that the heating processes are influenced by the topology of the magnetic field. Preferential heating is also evident, as the α particles tem-

For Peer Review

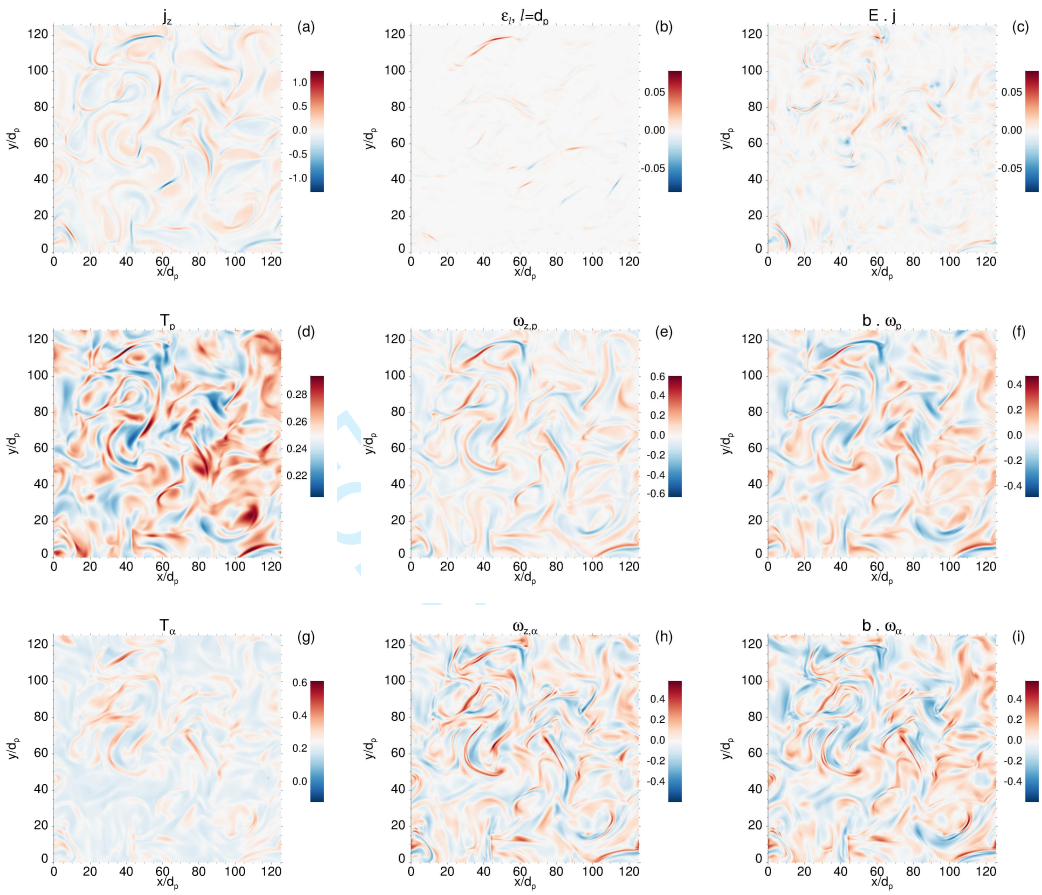

FIGURE 1. (Color online) 2D contour plots for the HVM multi-component simulation at $t = t^*$. (a) The out-of-plane total current density j_z; (b) the local energy transfer rate ϵ_{d_p}; (c) $\mathbf{E} \cdot \mathbf{j}$; (d) the proton temperature T_p; (e) the out-of-plane proton vorticity $\omega_{z,p}$; (f) $\mathbf{b} \cdot \omega_p$; (g) the α particle temperature T_α; (h) the out-of-plane α particle vorticity $\omega_{z,\alpha}$; and (i) $\mathbf{b} \cdot \omega_\alpha$.

perature is nearly twice that of the protons. Moreover, while the protons display roughly equal heating and cooling with respect to the initial temperature T_0, the α particles show predominant temperature increase.

Enhanced ion heating was recently observed in spatial regions nearby the peaks of the ion vorticity $\omega = \nabla \times \mathbf{v}$ (Servidio *et al.* 2015; Franci *et al.* 2016; Valentini *et al.* 2016). Previous studies have shown the association between viscous-like effects, velocity shears (Markovskii *et al.* 2006; Del Sarto *et al.* 2016) and vorticity (Huba 1996), including the dependence on the sign of $\mathbf{B_0} \cdot \omega$ (Parashar & Matthaeus 2016). In particular, it has been shown that the vorticity may enhance local kinetic effects, with a generalized resonance sign-dependence condition for the enhancement or reduction of the ion heating and temperature anisotropy (Parashar & Matthaeus 2016). In order to explore such correlation, the maps of the out-of-plane ion vorticities $\omega_{z,p}$ and $\omega_{z,\alpha}$, are shown in panels (e) and (h) of Figure 1. A pattern of small-scale vorticity structures can be observed, similar to the case of the current. However, a more complex topology is observed for the α particles vorticity, with the splitting of the structures in smaller filaments already observed in Hall-MHD turbulence (Martin 2013).

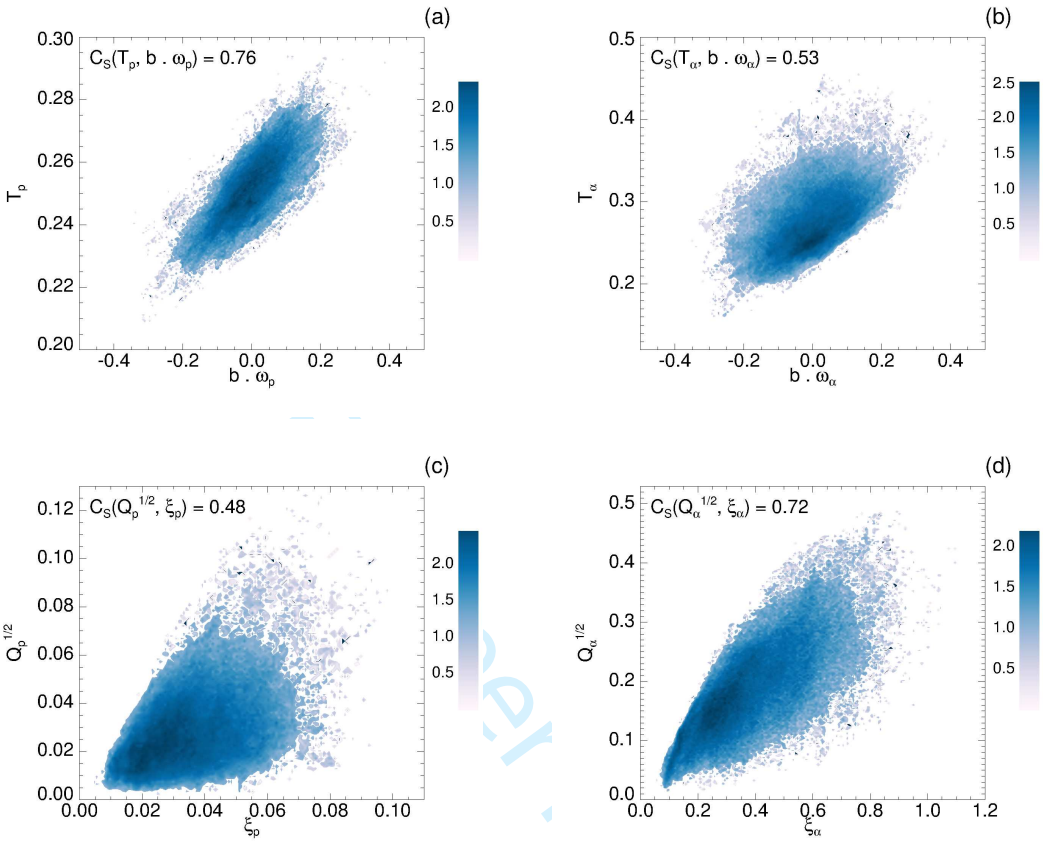

FIGURE 2. Joint probability distributions for (a) T_p and $\mathbf{b} \cdot \omega_p$; (b) T_α and $\mathbf{b} \cdot \omega_\alpha$; (c) $Q_p^{1/2}$ and ξ_p; (d) $Q_\alpha^{1/2}$ and ξ_α.

Finally, in panels (f) and (i) of Figure 1 we show the 2D contour plot of $\mathbf{b} \cdot \omega$ for both protons and α particles, respectively, where $\mathbf{b} = \mathbf{B} - \mathbf{B_0}$ indicates the magnetic field fluctuations. A behavior similar to ω_z is observed, so that both positive ω_z and $\mathbf{b} \cdot \omega$ correspond to increased temperature, for both ion species.

The overview of the numerical results of the HVM multi-species simulation given in Figure 1 highlights a general enhancement of the ion temperature related to the presence of thin current sheets. A more evident correlation is found with the ion out-of-plane vorticity ω_s and with $\mathbf{b} \cdot \omega_s$. To better appreciate the robustness of the observed correlation between T_s and $\mathbf{b} \cdot \omega_s$, in panel (a) e (b) of Figure 2 we show the average joint probability distributions $P(T_p, \mathbf{b} \cdot \omega_p)$ and $P(T_\alpha, \mathbf{b} \cdot \omega_\alpha)$, respectively. A good correlation is observed for both ion species, that we quantify through the nonlinear Spearman correlation coefficients, C_S, indicated in each panel of Figure 2. Correlations are stronger for protons $[C_S(T_p, \mathbf{b} \cdot \omega_p) = 0.76]$, than for α particles $[C_S(T_\alpha, \mathbf{b} \cdot \omega_\alpha) = 0.53]$. However, the correlation between the temperature and the out-of-plane vorticity (*i.e.*, the vorticity component parallel to the background magnetic field rather than to the magnetic fluctuations) is larger for the α particles: $C_S(T_p, \omega_{z,p}) = 0.49$ and $C_S(T_\alpha, \omega_{z,\alpha}) = 0.63$ (joint distributions are not shown for this case). The heating is thus better correlated with the out-of-plane vorticity for the α particles, but with the vorticity component parallel to

the local magnetic fluctuations for the protons. This may be related to the heavier α particles being slower than protons in following the magnetic field fluctuations.

The heating mechanisms are also correlated with strong deformation of the ion velocity distribution (Servidio *et al.* 2012; Valentini *et al.* 2016). For each ion species and in each point of the simulation domain, the non-Maxwellian measure can be defined as (Greco *et al.* 2012; Vasconez *et al.* 2015; Pucci *et al.* 2016; Valentini *et al.* 2017; Pezzi *et al.* 2017c):

$$\xi_s = \frac{1}{n_s}\sqrt{\int (f_s - g_s)^2 d^3v}. \tag{2.4}$$

The above scalar function measures the deviation of the observed distribution f_s from the associated Maxwellian g_s, which is built using the local density, bulk velocity and temperature. The latter quantity is also intimately related to the so-called velocity space cascade, recently observed in space plasmas (Servidio *et al.* 2017).

It is useful at this point to consider the agyrotropy of the pressure tensor, *i.e.* its departure from cylindrical symmetry around the local magnetic field direction. Non-gyrotropy is important as a known source of instabilities, and may help identifying spatial structures in the plasma (Scudder & Daughton 2008; Aunai *et al.* 2013; Swisdak 2016). For both ion species, given the 3×3 pressure tensor with elements P_{ij} in an arbitrary Cartesian system with coordinates (x, y, z), the measure of agyrotropy can be defined as the scalar (Swisdak 2016):

$$Q_s = 1 - \frac{4I_{2,s}}{(I_{1,s} - P_{\|,s})(I_{1,s} + 3P_{\|,s})}\ , \tag{2.5}$$

with $I_1 = P_{xx} + P_{yy} + P_{zz}$, and $I_2 = P_{xx}P_{yy} + P_{xx}P_{zz} + P_{yy}P_{zz} - (P_{xy}P_{yx} + P_{xz}P_{zx} + P_{yz}P_{zy})$. $P_\|$ here represents the parallel pressure, where we have omitted the subscript s for simplicity. A good correlation is observed between the non-gyrotropy of the ion pressure tensor, $Q_s^{1/2}$, and the non-Maxwellianity of the ion velocity, ξ_s, as shown in the joint probability distribution maps in panels (c) and (d) of Figure 2 for protons and α particles, respectively. This mechanism works better for α particles $[C_S(Q_\alpha^{1/2}, \xi_\alpha) = 0.72]$ with respect to protons $[C_S(Q_p^{1/2}, \xi_p) = 0.48]$, since deviations from Maxwellian are significantly stronger for the α particles than for protons.

Table 1 collects the Spearman correlation coefficients estimated for pairs of quantities for which $C_S \gtrsim 0.4$, namely if at least a significant moderate correlation is present. These also include the temperature anisotropy $A_s = T_{\perp,s}/T_{\|,s}$, defined for both ion species, an important diagnostic for kinetic processes and instabilities. In the Table, we have omitted the weakly correlated pairs, for which $C_S \lesssim 0.4$.

To summarize the results of the above analysis, larger values of the deformation of the ion velocity and of the pressure tensor agirotropy are recovered in spatial positions nearby the peaks of the ion vorticity and close to peaks of the current density. In these regions, differential heating and temperature anisotropy are also observed. Ion heating and kinetic effects are in general more strongly correlated with the vorticity than with the current density profile.

3. Local energy transfer rate in Vlasov-Maxwell simulations

3.1. *Properties of the local energy transfer rate*

Incompressible and isotropic MHD turbulence in plasmas can be described by the exact relation for the energy flux through the scales (see Equation 1.1). This Yaglom-like scaling

For Peer Review

Spearman Correlation Coefficients		
$(T_p, \omega_{z,p}) = 0.49$	$(T_p, \mathbf{b}\cdot\omega_p) = 0.76$	$(T_p, A_p) = 0.42$
$(T_\alpha, \omega_{z,p}) = 0.63$	$(T_\alpha, \mathbf{b}\cdot\omega_\alpha) = 0.53$	$(T_\alpha, A_\alpha) = 0.52$
$(A_p, \omega_{z,p}) = 0.45$	$(A_p, \mathbf{b}\cdot\omega_p) = 0.38$	$(Q_p^{1/2}, \xi_p) = 0.48$
$(A_\alpha, \omega_{z,\alpha}) = 0.57$	$(A_\alpha, \mathbf{b}\cdot\omega_\alpha) = 0.52$	$(Q_\alpha^{1/2}, \xi_\alpha) = 0.72$
$(\omega_{z,\alpha}, \omega_{z,p}) = 0.65$	$(\mathbf{b}\cdot\omega_\alpha, \mathbf{b}\cdot\omega_p) = 0.69$	$(\xi_{z,\alpha}, \xi_{z,p}) = 0.61$

TABLE 1. Nonlinear Spearman correlation coefficients, C_S, between pairs of quantities for which $C_S \gtrsim 0.4$. All quantities are estimated using the HMV simulation results at $t = t^*$.

law has been extensively tested in the solar wind, recovering very good agreements. The use of HVM multi-component simulation, described in Section 2, can provide a better understanding of the connection between the MHD turbulent cascade and the relative kinetic effects on the ion velocity distributions since the 'in situ' solar-wind measurements have several limitations.

In Figure 3, we present the validation of the PP law for the turbulent Vlasov simulation used in this work, as estimated by averaging Equation (1.2). In the range of scales roughly corresponding to the inertial range of MHD turbulence, *i.e.* for $2d_p \lesssim l \lesssim 10d_p$, the scaling of $-Y(l)$ is compatible with a linear law (Figure 3). This suggests that the turbulent energy cascade is well developed in such range, at the time t^* of the simulation. However, the limited extension of the inertial range does not allow a more precise and quantitative estimate (Parashar *et al.* 2015). It should be pointed out that the law as defined in Equation (1.1), without absolute value, is indicating the direction of the cascade towards small scales. The limited extension of the range observed in the HVM simulation may arise from several facts, which are physically meaningful. First, the system described here is size-limited due to computational constraints: the correlation length is limited to roughly $10d_p$ —relatively short as compared to the several decades of MHD turbulence commonly observed in the solar wind. Second, the PP law is exact only under the assumption of full isotropy, while our 2D simulation has a mean magnetic field. Third, the ion skin depth is a characteristic length of the system, which breaks the validity of the MHD law. A more precise description could be obtained in terms of the Hall-MHD version of the PP law (Andrés *et al.* 2018). This development is left for a future work. Fourth, in the derivation of these MHD-based scaling laws, isotropy of the pressure tensor is assumed, which does not hold in Vlasov turbulence. Finally, processes such as ion-cyclotron resonances and Landau damping might transfer free energy from the physical space to the velocity space, producing non-Maxwellian effects and, eventually, heating. All these caveats suggest that the analysis in terms of PP law and LET can only be meaningful for increments in the inertial range, $l > d_p$. **Therefore, part of our analysis will be performed using** $l = 2d_p$.

The local proxy $\epsilon_l(x, y)$ has been evaluated at different spatial scales l using the HVM simulation results. In Figure 4 we show the scalogram of the LET ϵ_l along a one-dimensional cut of the 2D spatial domain of the simulation. Note that a similar analysis has been performed for the PVI scalograms (Greco *et al.* 2016). Here we consider a diagonal path r, normalized to d_p, that crosses the simulation box several times. The

For Peer Review

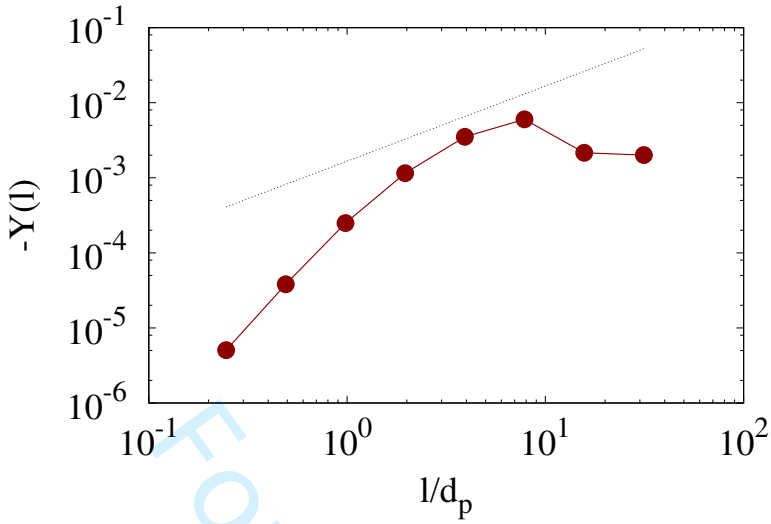

FIGURE 3. (Color online) Yaglom law validation for turbulent Vlasov simulation (red markers and dashed line). The averaged scaling $Y = (Y^+ + Y^-)/2$ is shown **using bi-logarithmic axes**. The black dotted line represents an example of linear scaling, and is shown for reference only.

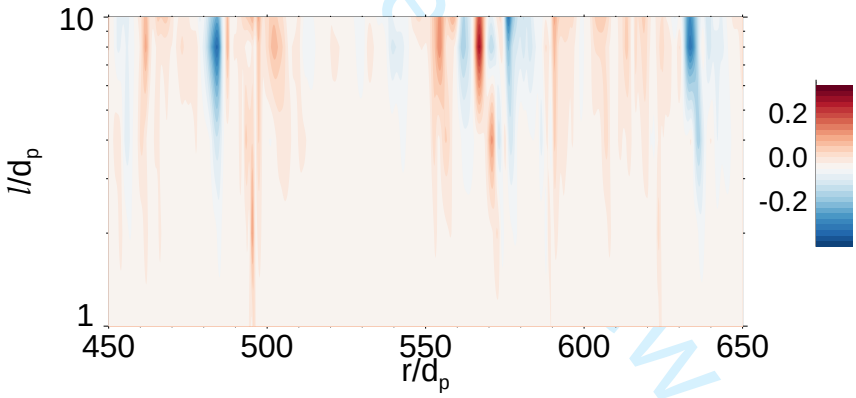

FIGURE 4. (Color online) The scalogram of LET ϵ_l, plotted as color map at different scales l/d_p, estimated at different positions r/d_p along a one-dimensional cut of the simulation domain. The alternate positive and negative energy transfer regions are evident.

channels of energy being transferred across scales are clearly visible, and reveal the complex, interwoven pattern of positive and negative flux that determines the neat energy flux (Coburn *et al.* 2014; Sorriso-Valvo *et al.* 2018).

In order to characterize the statistical properties of the local energy transfer rate, in Figure 5, we show the probability distribution functions (PDFs) of the negative (left panel) and positive (central panel) standardized LET values (*i.e.*, $\epsilon_l(x, y)$ has been rescaled to have zero mean and unit standard deviation), for three different scales, namely $l = d_p$ (blue diamonds), $4d_p$ (green triangles) and $8d_p$ (red circles). In agreement with the PP law, for a given scale the positive tails are considerably higher and shallower than the negative ones, indicating the neat energy flux corresponding to the direct turbulent

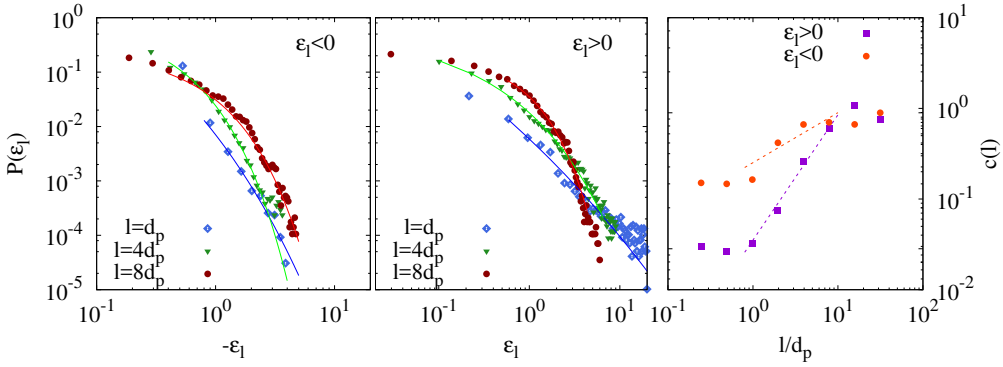

FIGURE 5. (Color online) In the left panel, the probability distribution functions (PDFs) of the standardized, negative $\epsilon_l(x,y)$ are shown for three different scales, namely $l = d_p$ (blue diamonds), $4d_p$ (green triangles) and $8d_p$ (red circles), using logarithmic axes. In the central panel, the PDFs of positive $\epsilon_l(x,y)$ are shown for the same scales, with the same symbols. In both panels, the different lines are the stretched exponential fits, obtained through a standard least-χ^2 procedure. The right panel shows the scaling properties of the curvature parameter $c(l)$, for the positive (violet squares) and negative (orange circles) tails of the PDFs. The inertial range power-law fits are also indicated as dashed lines, the scaling exponents being respectively $\gamma_+ = 0.92$ and $\gamma_- = 0.37$.

energy cascade towards small scales. This is clearly visible from the PDFs represented in Figure 5.

Both positive and negative PDFs behave roughly as stretched exponential functions $\sim \exp\left(-b\epsilon_l^c\right)$, where c is the parameter that controls the shape of the distribution tails. In particular, $c = 2$ indicates a Gaussian tail, $c = 1$ an exponential tail, and for $c \to 0$ the tail approaches a power-law. The curvature parameter c, obtained from the fit at each scale, is shown in the right panel of Figure 5. Starting from the exponential value $c \sim 1$ at large scales (say for $l \gtrsim 10d_p$), its value decreases with the scales, indicating the formation of highly localized small-scale structures, typical of intermittency. The two tails of the PDFs have different scaling, so that the positive tail has a more evident, faster decay than the negative tail. Such difference quantitatively confirms the imbalance already observed through the PDF shape. In the range corresponding to the MHD inertial range, the scaling of c for the positive tail is well described by a power-law $c_\pm^\gamma$, with exponent $\gamma_+ \sim 0.92 \pm 0.06$. For the negative tail, the scaling is less evident, but can be considered compatible with a power law with exponent $\gamma_- \sim 0.37 \pm 0.13$. This confirms that the numerical simulation has reached a stage of fully developed turbulence, with a strongly intermittent energy cascade, whose characteristics are well captured by the LET. Note that a similar behavior has been recently observed in solar wind measurements (Sorriso-Valvo *et al.* 2018). At smaller scales, for $l \lesssim d_p$, the parameter seems to reach a limiting value for both the positive and negative tails, indicating the saturation of intermittency. In this short range of scales, the positive tail of the PDF is described by $c \sim 0.1$, closer to power-law decay. The negative tail converges towards a slightly larger value $c \sim 0.3$, indicating a faster than power-law decay, and confirming once more the quantitative difference between positive and negative energy transfer rate.

3.2. *Conditioned analysis of kinetic quantities*

After establishing the statistical properties of the LET in our hybrid simulation, we have performed the conditioned average analysis proposed by Osman *et al.* (2012), and recently performed using the LET (Sorriso-Valvo *et al.* 2018). The conditioned analysis

For Peer Review Only

is designed to highlight the existence of robust features in the data that might be hidden by the turbulent fluctuations. To this goal, we have selected different values of threshold θ_{d_p} of the LET ϵ_{d_p}, estimated at the bottom of the inertial range $l \simeq 2d_p$, to identify locations associated with large energy flux at the end of the fluid-like nonlinear turbulent cascade.

Then, for each threshold, some of the variables described in Section 2 have been averaged only in those locations where the LET overcomes the threshold: $\epsilon_{d_p} \geq \theta_{d_p}$ for positive thresholds (cascade towards smaller scales), and $\epsilon_{d_p} \leq \theta_{d_p}$ for negative thresholds (cascade towards higher scales). This gives the conditioned averaged values, for example $\langle T_p|\theta_{d_p}\rangle$ in the case of the proton temperature.

Through the above procedure, the turbulent fluctuations are all averaged to their mean value, except where systematic variations are present. The same procedure is repeated using all the points located at a given distances δ from the location of large LET, and for different values of δ. This provides the average profile of the physical quantities in the vicinity of the bursts of energy flux, as a function of the distance from the LET burst. By repeating the same analysis using different thresholds, it is then possible to determine the role of the energy flux in the robust modification of the physical quantities.

The 12 panels of Figure 6 show the conditioned average profiles obtained using the HVM simulation results, for some of the physical quantities described in Section 2 and indicated in each panel. The average has been computed up to a distance $\delta = 12d_p$ from the LET peaks. For each panel, the different line styles refer to the different threshold values, as listed at the bottom of the figure. All curves have been vertically shifted for clarity, and are therefore given in arbitrary units. The dotted horizontal line has the only purpose of separating the positive from the negative threshold values. The figure shows that most of the variables have a clear enhancement at $\delta = 0$ in the positive LET peak cases, which is more evident for larger threshold values. At the same time, in most cases the negative LET peaks are associated with a reduction of the conditioned average, again more evident for larger negative thresholds. This observation generally suggests that kinetic processes are more effective within a few d_p from the intermittent structures, or more precisely from the locations where the fluid-scale turbulent cascade has produced a larger flux of energy.

A more detailed look at the individual panels of Figure 6 can provide information that may help uncovering the kinetic processes occurring in the simulation. Panel A shows that the off-plane current j_z is not well co-located with the positive LET structures, as the conditioned average profiles show a weak peak near $\delta \simeq 3d_p$. **Note that conditioning the average j_z to large values of the LET estimated at the smallest scale in the simulation results in larger correlations than at $l = 2d_p$. This is to be expected, and possibly trivial, as the contribution to the LET of the LET term including Δb^2 (strongly correlated to j_z) and Δv^2 (strongly correlated to ω_z) would dominate, since the other term (including the $\Delta v \cdot \Delta b$ correlations) becomes less meaningful.** On the contrary, regions of strong negative LET are associated to smaller current, as evident from the bottom part of panel A. This could arise from the fact that negative LET structures are associated with regions where the turbulent production of small scales is locally inhibited, indicating possible equilibrium-like patterns, that results from a process of suppression of nonlinearity (Servidio *et al.* 2008).

In panels B and C, the average proton and α particle vorticity peak at large positive LET locations, and, as for the current, is minimal for large negative LET. **This observation confirms previous results, obtained using particle-in-cell simulations, which show that correlations between vorticity structures and kinetic**

For Peer Review

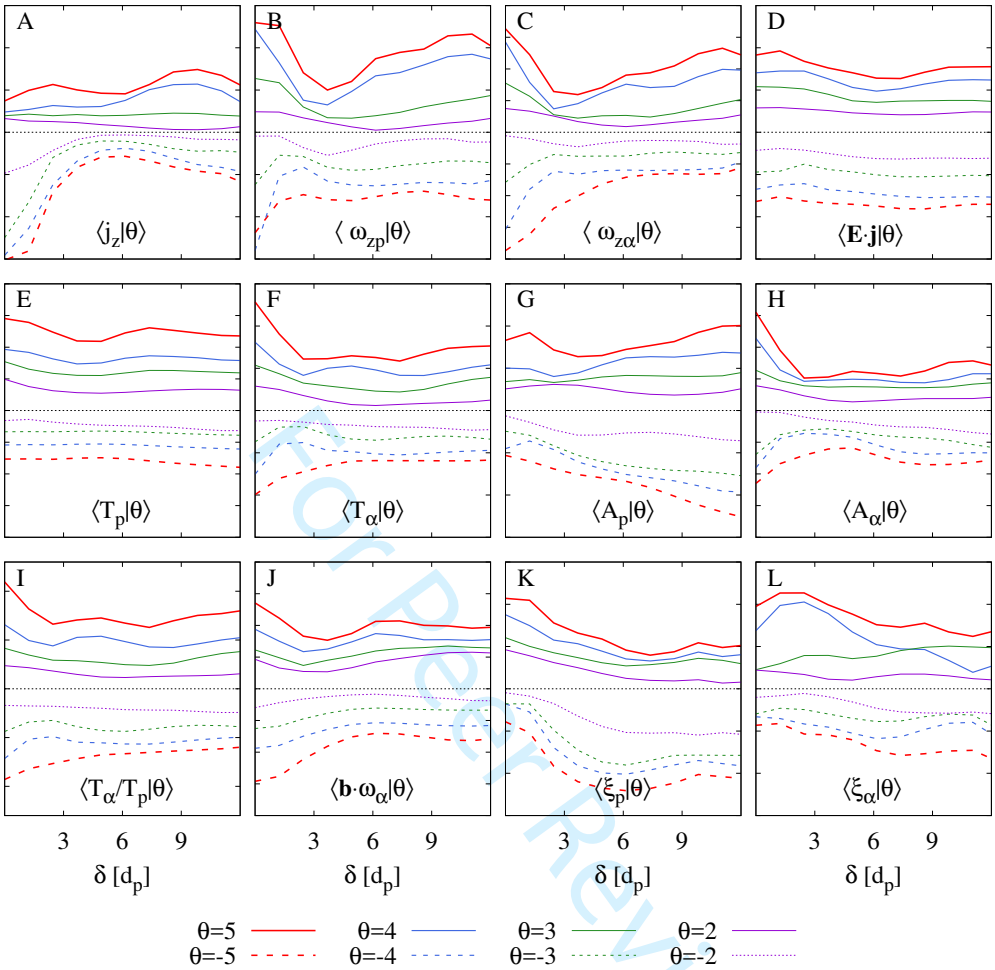

FIGURE 6. (Color online) Conditioned averaged quantities as a function of the distance from the peak of the LET, estimated at the scale $l \simeq 2d_p$, for four positive and four negative LET threshold values θ_{d_p} (coded in different line colors, as indicated at the bottom of the Figure). Each panel refers to one of the physical quantities (see Section 2, given in the legend located at the bottom of the panel). All curves have been vertically shifted for clarity, and are thus presented in arbitrary units. In each panel, the curves for larger positive thresholds (full lines) are those shown at upper positions, and the larger negative thresholds (dashed lines) are shown at lower positions. The dotted horizontal line has the sole purpose of separating the curves relative to positive (above the line) and negative (below the line) thresholds.

For Peer Review

features are stronger than for the current structures (Parashar & Matthaeus 2016).

Panel D shows that the exchange of energy between particles and fields, represented here through the quantity $\mathbf{E} \cdot \mathbf{j}$, is weakly enhanced near the LET positive peaks, but is relatively unaffected by the presence of negative LET peaks. This is in good agreement with previous works, where it has been shown that locally the cascade produces narrow heating and dissipation patterns (Karimabadi *et al.* 2013).

Panels E and F display enhanced temperature near the positive LET peaks for both species, which extends up $\delta \sim 2$–$3d_p$ from the peaks. For the α particles, there is indication

of colder temperature near the large negative LET points, which highlights the possible presence of a differential heating processes of the two species (Kasper *et al.* 2008; Maruca *et al.* 2012).

Panels G and H show the conditioned profiles of the temperature anisotropy A_s. In panel G, the proton temperature anisotropy is only weakly affected by large positive energy transfer, while a general anisotropy increase can be observed in correspondence with large negative LET. On the contrary, as can be seen in panel H, the α particle temperature anisotropy increases (decrease) near the large positive (negative) LET structures. In this case, the LET dependence is similar for the temperature anisotropy and for the total temperature. This suggests that the presence of large turbulent energy transfer increases predominantly the perpendicular temperature, indicating for example the possible role of ion-cyclotron or mirror instabilities (Matteini *et al.* 2013).

Panel I quantifies the strong enhancement of the temperature ratio T_α/T_p near the sites of strong positive energy transfer, and the corresponding decrease at the negative LET peaks. This plot magnifies the difference in the conditional averaged temperature for the two species, seen in panels E and F, and confirms the relevance of differential heating at the sites of strong turbulent activity.

Panel J shows that the quantity $\mathbf{b} \cdot \omega_s$ has similar conditioned averages as for the vorticity (see panels B and C), for both protons (not shown) and α particles.

Finally, panels K and L show that the parameter ξ_s, quantifying the general deviation from Maxwellian VDF, is clearly larger at both positive and negative LET structures, and for both ion species. This last observation confirms that the kinetic processes resulting in modification of the ion VDFs are predominantly seen in the proximity of the locations with enhanced turbulent energy flux, where free energy is available for small-scale processes to occur. Additionally, it suggests that regions characterized by absent or reduced direct energy transfer towards small scales (large negative LET) are also characterized by the presence of robustly non-Maxwellian VDF. Whether this indicates that kinetic effect may provide feedback to the larger scales through some form of inverse cascade remains an open question that deserves further analysis.

It is interesting but not surprising to note that, for most of the physical quantities studied here, the observed peaks extend to approximately 2–3d_p around the LET structures. This indicates that the effects of the kinetic features are typically smeared out within such range.

4. Conclusions

Exploring the details of the cross-scale connections between the MHD turbulent energy cascade and the small-scale kinetic processes is an important key to understand the role of dissipation mechanisms in collisionless plasmas (Schwartz *et al.* 2011; Alexandrova *et al.* 2013; Chen 2016). Numerical simulations can provide important insight on general processes, in particular when experimental systems and observations are not easily controlled.

In this article, we have presented the analysis of one snapshot in the quasi-steady state turbulence of a two-dimensional Hybrid Vlasov-Maxwell numerical simulation (HVM), with the inclusion of α particles. The range of scales that have been investigated includes both the fluid range, where MHD turbulence transfers energy across scales, and the sub-ion range, where kinetic effects dominate the dynamics. This multi-scale investigation allows to explore the role of the turbulent energy that reaches the typical ion scales in

For Peer Review

highly localized regions of space (both in the form of coherent structures and of correlated fluctuations) and the kinetic processes occurring at small scales. The former is represented by means of a proxy of the Local Energy Transfer rate (LET), whose heuristic definition is based on the linear scaling laws of the mixed third-order moment of the MHD fluctuations, **and which carries more details on the type of fluctuations associated with the energy transfer with respect to other proxies (***e.g.* **the PVI)**. The latter are described here through several quantities that can be related to kinetic processes, as for example the ion temperature and its anisotropy with respect to the magnetic field direction, or an index of deviation from Maxwellian particle velocity distribution.

We have initially described the correlations between such kinetic quantities, first by visually comparing their maps, then by looking at some examples of joint probability distributions of such quantities pairs, and finally by estimating the nonlinear correlation coefficients between all the pairs. Several diagnostics show significant correlation. For example, the ion vorticity and the associated temperature show moderate correlation for both species, confirming previous observations that the temperature is enhanced in correspondence of vorticity structures (Servidio *et al.* 2015; Franci *et al.* 2016; Valentini *et al.* 2016; Parashar & Matthaeus 2016). The deviation from Maxwellian (Servidio *et al.* 2012; Valentini *et al.* 2016) is also very well correlated with the pressure tensor anisotropy, revealing its relevant contribution in determining such deviation.

We have then analyzed the statistical properties of the energy transfer rate in HVM turbulence. The domain-averaged third-order moment suggests that the turbulent cascade might be fully developed in the range approximately between $\sim 2d_p$ and $\sim 10d_p$, where the measured energy flux is compatible with linear scaling. A direct cascade of energy is present (the negative sign of the third-order moment Y), in agreement with the expectations for turbulence in the MHD inertial range of scales. However, looking at the space-scale distribution of the local contributions to such scaling law, it is clear that both positive and negative energy fluxes exist, and are in comparable quantity, all across the simulation domain, the negative sign being the global balance between those.

The scaling properties of the LET were modeled in terms of stretched exponential distributions, which provided a satisfactory description of the PDFs at all scales. The imbalance between positive and negative values of ϵ are well described by the asymmetry of their distributions. Moreover, the shape parameter of the fitted distributions shows power-law scaling in the inertial range, in agreement with previous observations of solar wind turbulence (Sorriso-Valvo *et al.* 2018) and confirming the reliability of the proxy for the description of the turbulence properties.

Finally, we have explored the presence of correlations between the LET and the quantities described before. To this aim, we have calculated the conditionally averaged profile of each of those quantity, around the locations where the LET exceeds some given thresholds (Osman *et al.* 2012; Sorriso-Valvo *et al.* 2018). This analysis may provide more detailed information that can help understand which kinetic processes are responsible for the removal (or transformation) of the turbulent energy from the system. These profiles shows that most of the physical quantities related to "dissipative" or kinetic processes are enhanced near regions of large positive LET, indicating a large flux of energy towards small scales. Conversely, these are often reduced near strong negative LET, likely associated to energy being transferred towards large scales, and thus indicating less availability of energy in the kinetic range.

Our results suggest, for example, that peaks of turbulent energy transfer are associated with enhanced temperature. More in particular, the perpendicular temperature increases near the high LET locations, indicating the possible role of ion-cyclotron or mirror in-

For Review Only

stabilities (Matteini *et al.* 2013). The typical size of the region where the enhancement is observed is, for most quantities, of the order of 2–3d_p, while at larger distance their persistent fluctuations are averaged out. It is also clear from the analysis that the vorticity is a better tracer of energy availability than the current density (Servidio *et al.* 2015; Franci *et al.* 2016; Parashar & Matthaeus 2016; Valentini *et al.* 2016), and that correlations are more evident for the α particles than for protons (Valentini *et al.* 2016). Finally, deviations from Maxwellian VDF are evident for both positive and negative peaks of LET, an interesting feature that deserves further analysis.

The study of the local properties of the turbulent cascade can be a valuable tool for the exploration of the kinetic range processes in space plasmas. The validation of its use in numerical simulations provided in this work suggests its possible use with the recently available high-quality plasma measurements in the solar wind and in the magnetosphere, provided by the Multiscale Magnetospheric mission MMS (Burch *et al.* 2016a). Extension to more complete descriptions of the energy transfer rate could be also used, allowing, for example, to examine the actual role played by compressive effects (Carbone 2009; Andrés *et al.* 2018).

For Peer Review

Acknowledgements

This work has been partly supported by the Agenzia Spaziale Italiana under the Contract No. ASI-INAF 2015-039-R.O "Missione M4 di ESA: Partecipazione Italiana alla fase di assessment della missione THOR" and by the International Space Science Institute (ISSI) in the framework of International Team 504 entitled "Current Sheets, Turbulence, Structures and Particle Acceleration in the Heliosphere". L.S.-V., D.P., S.S. and I.Z. acknowledge support from the Faculty of the European Space Astronomy Centre (ESAC). Numerical simulations here discussed have been run on the Newton parallel machine at the University of Calabria (Italy).

REFERENCES

Alexandrova, O., Carbone, V., Veltri, P. & Sorriso-Valvo, L. 2008 Small-scale energy cascade of the solar wind turbulence. *The Astrophysical Journal* **674**, 1153.

Alexandrova, O., Chen, C.H.K., Sorriso-Valvo, L., Horbury, T.S. & Bale, S.D. 2013 Solar wind turbulence and the role of ion instabilities. *Space Science Reviews* **178**, 101.

Andrés, N., Galtier, S., Sahraoui, F. 2018 Exact law for homogeneous compressible Hall magnetohydrodynamics turbulence. *Physical Review E* **97**, 013204.

Andrés, N. & Sahraoui, F. 2017 Alternative derivation of exact law for compressible and isothermal magnetohydrodynamics turbulence. *Physical Review E* **96**, 053205.

Araneda, J.A., Maneva, Y. & Marsch, E. 2009 Preferential Heating and Acceleration of alpha Particles by Alfven-Cyclotron Waves. *Physical Review Letters* **102**, 175001.

Aunai, N., Hesse, M. & Kuznetsova, M. 2013 Electron nongyrotropy in the context of collisionless magnetic reconnection. *Physics of Plasmas* **20**, 092903.

Breuillard, H., Yordanova, E., Vaivads, A. & Alexandrova, O. 2016 The effects of kinetic instabilities on small-scale turbulence in Earth's magnetosheath. *The Astrophysical Journal* **829**, 54.

Bruno, R., Bavassano, B., Pietropaolo, E., Carbone, V., & Veltri, P. 1999 Effects of intermittency on interplanetary velocity and magnetic field fluctuations anisotropy. *Geophysical Research Letters* **26**, 3185–3188.

Bruno, R. & Carbone, V. 2013 The solar wind as a turbulence laboratory. *Living Reviews in Solar Physics* **10**, 1.

Burch, J.L., Moore, T.E., Torbert, R.B., Giles, B.L. 2016 Magnetospheric Multiscale Overview and Science Objectives. *Space Sci. Rev.* **199**, 5.

Burch, J.L., Torbert, R.B., Phan, T.D., Chen, L.-J., Moore, T.E., Ergun, R.E.,

Eastwood, J.P., Gershman, D.J., Cassak, P.A., Argall, M.R., Wang, S., Hesse, M., Pollock, C.J., Giles, B.L., Nakamura, R., Mauk, B.H., Fuselier, S.A., Russell, C.T., Strangeway, R.J., Drake, J.F., Shay, M.A., Khotyaintsev, Yu.V., Lindqvist, P.-A., Marklund, G., Wilder, F.D., Young, D.T., Torkar, K., Goldstein, J., Dorelli, J.C., Avanov, L.A., Oka, M., Baker, D.N., Jaynes, A.N., Goodrich, K.A., Cohen, I.J., Turner, D.L., Fennell, J.F., Blake, J.B., Clemmons, J., Goldman, M., Newman, D., Petrinec, S.M., Trattner, K.J., Lavraud, B., Reiff, P.H., Baumjohann, W., Magnes, W., Steller, M., Lewis, W., Saito, Y., Coffey, V. & Chandler, M. 2016 Electron-scale measurements of magnetic reconnection in space. *Science* **352**, 6290.

Burlaga, L. F. 1991 Intermittent turbulence in the solar wind. *Journal of Geophysical Research* **96**, 5847.

Chasapis, A., Retinò, A., Sahraoui, F., Vaivads, A., Khotyaintsev, Yu.V., Sundkvist, D., Greco, A., Sorriso-Valvo, L. & Canu, P. 2015 Thin current sheets and associated electron heating in turbulent space plasma. The Astrophysical Journal Letters **804**, L1.

Camporeale, E. & Burgess, D. 2011 The dissipation of solar wind turbulent fluctuations at electron scales. *The Astrophysical Journal* **730**, 114.

Carbone V., Marino, R., Sorriso-Valvo, L., Noullez, A., & Bruno, R. 2009 Scaling laws of turbulence and heating of fast solar wind: the role of density fluctuations. *Physical Review Letters* **103** 115001.

Cerri, S.S., Califano, F., Jenko, F., Told, D., & Rincon, F. 2016 Subproton-scale cascades in solar wind turbulence: driven hybrid-kinetic simulations. *The Astrophysical Journal Letters* **822**, L12.

Cerri, S.S., Servidio, S., & Califano, F. 2017 Kinetic cascade in solar-wind turbulence: 3D3V hybrid-kinetic simulations with electron inertia. *The Astrophysical Journal Letters* **846**, L18.

Cerri, S.S., Kunz, M.W. & Califano, F. 2018 Dual phase-space cascades in 3D hybrid-Vlasov-Maxwell turbulence. Accepted to *The Astrophysical Journal Letters*. arXiv:1802.06133

Chasapis, A., Matthaeus, W.H., Parashar, T.N., LeContel, O, Retinò, A., Breuillard, H., Khotyaintsev, Yu.V., Vaivads, A., Lavraud, B., Eriksson, E., Moore, T.E., Burch, J.L., Torbert, R.B., Lindqvist, P.-A., Ergun, R.E., Marklund, G., Goodrich, K.A., Wilder, F.D., Chutter, M., Needell, J., Rau, D., Dors, I., Russell, C.T., Le, G., Magnes, W., Strangeway, R.J., Bromund, K.R., Leinweber, H.K., Plaschke, F., Fischer, D., Anderson, B.J., Pollock, C.J., Giles, B.L., Paterson, W.R., Dorelli, J., Gershman, D.J., Avanov, L. & Saito Y. 2017 Electron heating at kinetic scales in magnetosheath turbulence. The Astrophysical Journal **836**, 247.

Chen, C.H.C. 2016 Recent progress in astrophysical plasma turbulence from solar wind observations. *Journal of Plasma Physics* **82**, 535820602.

Chen, C.H.C., Matteini, L., Schekochihin, A.A., Stevens, M.L., Salem, C.S., Maruca, B.A., Kunz, M.W. & Bale, S.D. 2016 Multi-species measurements of the firehose and mirror instability thresholds in the solar wind. *The Astrophysical Journal Letters* **825**, L26.

Coburn, J.T., Smith, C.W., Vasquez, B.J., Forman, M.A., & Stawarz, J.E. 2014 Variable cascade dynamics and intermittency in the solar wind at 1 AU. *The Astrophysical Journal* **786**, 52.

Del Sarto, D., Pegoraro, F. & Califano, F. 2016 Pressure anisotropy and small spatial scales induced by velocity shear. *Physical Review E* **93**, 053203.

Farge, M. 1992 Wavelet transfroms and their applications to turbulence. *Annual Review of Fluid Mechanics* **24**, 395.

Franci, L., Verdini, A., Matteini, L., Landi, S. & Hellinger, P. 2015 Solar wind turbulence from MHD to sub-ion scales: high resolution hybrid simulations. *The Astrophysical Journal Letters* **804**, L39.

Franci, L., Hellinger, P., Matteini, L., Verdini, A. & Landi, S. 2016 in *SOLAR WIND 14, Proc. Fourteenth Int. Solar Wind Conf. 1720*, ed. L. Wang et al. (New York: AIP) 040003

Franci, L., Landi, S., Verdini, A., Matteini, L., & Hellinger, P. 2018 Solar wind turbulent cascade from MHD to sub-ion scales: large-size 3D hybrid particle-in-cell simulations. *The Astrophysical Journal* **853**, 26.

For Peer Review

Frisch, U.P. 1995 *Turbulence: the legacy of A.N. Kolmogorov*, (Cambridge Univ. Press).

Greco, A., Chuychai, P., Matthaeus, W.H., Servidio, S. & Dimitruk, P. 2008 Intermittent MHD structures and classical discontinuities. *Geophysical Research Letters* **35**, L19111.

Greco, A. & Perri, S. 2014 Identification of high shear and compressive discontinuities in the inner heliosphere. *The Astrophysical Journal* **784**, 163.

Greco, A., Perri, S., Servidio, S., Yordanova, E., & Veltri, P. 2016 The Complex Structure of Magnetic Field Discontinuities in the Turbulent Solar Wind. *The Astrophysical Journal Letters* **823**, L39.

Greco, A., Valentini, F., Servidio, S. & Matthaeus, W.H. 2012 Inhomogeneous kinetic effects related to intermittent magnetic discontinuities. *Physics Review E* **86**, 066405.

Groselj, D., Cerri, S.S., Navarro, A.B., Willmott, C., Told, D., Loureiro, N.F., Califano, F., & Jenko, F. 2017 Fully Kinetic versus Reduced-kinetic Modeling of Collisionless Plasma Turbulence. *The Astrophysical Journal* **847**, 28.

Haggerty, C. C., Parashar, T. N., Matthaeus, W. H., Shay, M. A., Yang, Y., Wan, M., Wu, P., & Servidio, S. 2017 Exploring the statistics of magnetic reconnection X-points in kinetic particle-in-cell turbulence. *Physics of Plasmas* **24**, 102308.

Howes, G. G. 2016 The Dynamical Generation of Current Sheets in Astrophysical Plasma Turbulence. *The Astrophysical Journal Letters* **827**, L28.

Howes, G. G., McCubbin, A. J., & Klein, K. G. 2018 Spatially localized particle energization by Landau damping in current sheets produced by strong Alfvn wave collisions. *Journal of Plasma Physics* **84**, 905840105.

Huba, J. 1996 The KelvinHelmholtz instability: Finite Larmor radius magnetohydrodynamics. *Geophysical Research Letters* **23**, 2907.

Karimabadi, H., Roytershteyn, V., Wan, M., Matthaeus, W. H., Daughton, W., Wu, P., Shay, M., Loring, B., Borovsky, J., Leonardis, W., Chapman, S. C., & Nakamura, T. K. M. 2013 Coherent structures, intermittent turbulence, and dissipation in high-temperature plasmas. *Physics of Plasmas* **20**, 012303.

Kasper, J.C., Lazarus, A.J. & Gary, S. P. 2008 Hot solar-wind helium: direct evidence for local heating by Alfvn-cyclotron dissipation. *Physical Review Letters* **101**, 261103.

Kiyani, K.H., Chapman, S.C., Khotyaintsev, Yu.V., Dunlop, M.W. & Sahraoui, F 2009 Global scale-invariant dissipation in collisionless plasma turbulence. *Physical Review Letters* **103**, 075006.

Lion, S., Alexandrova, O. & Zaslavsky, A. 2016 Coherent events and spectral shape at ion kinetic scales in fast solar wind turbulence. *The Astrophysical Journal* **824**, 47.

MacBride, B.T., Forman, M.A. & Smith, C.W. 2005 In: Fleck, B., Zurbuchen, T.H., Lacoste, H. (eds.). *Solar Wind 11/SOHO 16, Connecting Sun and Heliosphere* (ESA Special Publication 592. 613)

MacBride, B.T., Smith, C.W. & Forman, M.A. 2008 The turbulent cascade at 1AU: energy transfer and the third-order scaling for MHD. *The Astrophysical Journal* **679**, 1644.

Maneva, Y.G., Vinas, A.F., Moya, P.S., Wicks, R., & Poedts, S. 2015 Dissipation of parallel and oblique Alfvén-cyclotron waves — implications for heating of alpha particles in the solar wind. *The Astrophysical Journal* **814**, 33.

Marino, R., Sorriso-Valvo, L., Carbone, V., Noullez, A., Bruno, R. & Bavassano, B. 2008 Heating the solar wind by a magnetohydrodynamic turbulent energy cascade. *The Astrophysical Journal Letters* **667**, L71.

Marino, R., Sorriso-Valvo, L., D'Amicis, R., Carbone, V., Bruno, R. & Veltri, V. 2012 On the occurrence of the third-order scaling in high latitude solar wind. *The Astrophysical Journal* **750**, 41.

Markovskii, S.A., Vasquez, B.J., Smith, C.W. & Hollweg, J.V. 2006 Dissipation of the perpendicular turbulent cascade in the solar wind. *The Astrophysical Journal* **639**, 1177.

Marsch, E. & Tu, C.-Y. 1997 Intermittency, non-Gaussian statistics and fractal scaling of MHD fluctuations in the solar wind. *Nonlinear Processes in Geophysics* **4**, 101.

Marsch, E. 2006 Kinetic physics of the solar corona and solar wind. *Living Reviews in Solar Physics* **3**, 1.

Martin, L.N., De Vita, G., Sorriso-Valvo, L., Dimitruck, P., Nigro, G., Primavera,

For Peer Review

L., and Carbone, V. 2013 Cancellation properties in Hall magnetohydrodynamics with a strong guide magnetic field. *Physical Review E* **88**, 063107.

Maruca, B.A, Kasper, J.C. & Gary, , S. P. 2012 Instability-drive limits on helium temperature anisotropy in the solar wind: observations and linear Vlasov analysis. *The Astrophysical Journal* **748**, 137.

Matteini, L., Hellinger, P., Goldstein, B. E., Landi, S., Velli, M. & Neugebauer, M. 2013 Signatures of kinetic instabilities in the solar wind. *Journal of Geophysical Reserch: Space Physics* **118**, 2771.

Osman, K.T., Matthaeus, W.H., Greco, A. & Servidio, S. 2011 Evidence for inhomogeneous heating in the solar wind. *The Astrophysical Journal Letters* **727**, L11.

Osman, K.T., Matthaeus, W.H., Hnat, B. & Chapman, S.C. 2012 Kinetic signatures and Intermittent turbulence in the solar wind plasma. *Physical Review Letters* **108**, 261103.

Parashar, T.N., Shay, M.A., Cassak, P.A. & Matthaeus, W.H. 2009 Kinetic dissipation and anisotropic heating in a turbulent collisionless plasma. *Physics of Plasmas* **16**, 032310.

Parashar, T.N., Matthaeus, W.H., Shay, M.A., & Wan, M. 2015 Transition from kinetic to MHD behavior in a collisionless plasma. *The Astrophysical Journal* **811**, 112.

Parashar, T.N. & Matthaeus, W.H. 2016 Propinquity of current and vortex structures: effects on collisionless plasma heating. *The Astrophysical Journal* **832**, 57.

Perrone, D., Valentini & Veltri, P. 2011 The role of alpha particles in the evolution of the solar-wind turbulence toward short spatial scales. *The Astrophysical Journal* **741**, 43.

Perrone, D., Valentini, F., Servidio, S., Dalena, S. & Veltri, P. 2013 Vlasov simulations of multi-ion plasma turbulence in the solar wind. *The Astrophysical Journal* **762**, 99.

Perrone, D., Bourouaine, S., Valentini, F., Marsch, E. & Veltri, P. 2014 Generation of temperature anisotropy for alpha particle velocity distributions in solar wind at 0.3 AU: Vlasov simulations and Helios observations. *Journal of Geophysical Research: Space Physics* **119**, 2400.

Perrone, D., Valentini, F., Servidio, S., Dalena, S. & Veltri, P. 2014 Analysis of intermittent heating in a multi-component turbulent plasma. *The European Physical Journal D* **68**, 209.

Perrone, D., Alexandrova, O., Mangeney, A., Maksimovic, M., Lacombe, C., Rakoto, V., Kasper, J.C. & Jovanovic, D. 2016 Compressive coherent structures at ion scales in the slow solar wind. *The Astrophysical Journal* **826**, 196

Perrone, D., Alexandrova, O., Roberts, O.W., Lion, S., Lacombe, C., Walsh, A., Maksimovic, M., & Zouganelis, I. 2017 Coherent structures at ion scales in fast solar wind: Cluster observations. *The Astrophysical Journal* **849**, 49

Peyret, R. & Taylor, T.D. 1986 *Computational Methods for Fluid Flow* (New York: Springer)

Pezzi, O., Valentini, F., Perrone, D. & Veltri, P. 2013 Eulerian simulations of collisional effects on electrostatic plasma waves. *Physics of Plasmas* **20**, 092111.

Pezzi, O., Valentini, F., Perrone, D. & Veltri, P. 2014 Erratum: "Eulerian simulations of collisional effects on electrostatic plasma waves" [Phys. Plasmas 20, 092111 (2013)] *Physics of Plasmas* **21**, 019901.

Pezzi, O., Valentini, F. & Veltri, P. 2015(a) Collisional Relaxation: Landau versus Dougherty operator. *Journal of Plasma Physics* **81**, 305810107.

Pezzi, O., Valentini, F. & Veltri, P. 2015 Nonlinear regime of electrostatic waves ropagation in presence of electron-electron collisions. *Physycs of Plasmas* **22**, 042112.

Pezzi, O., Valentini, F. & Veltri, P. 2016 Collisional relaxation of fine velocity structures in plasmas. *Physical Review Letters* **116**, 145001.

Pezzi, O., Parashar, T.N., Servidio, S., Valentini, F., Vásconez, C.L., Yang, Y., Malara, F., Matthaeus, W.H. & Veltri, P. 2017 Revisiting a classic: the Parker-Moffatt problem. *The Astrophysical Journal* **834**, 166.

Pezzi, O., Malara, F., Servidio, S., Valentini, F., Parashar, T.N., Matthaeus, W.H. & Veltri, P. 2017 Turbulence generation during the head-on collision of Alfvénic wave packets. *Physical Review E* **96**, 023201.

Pezzi, O., Parashar, T.N., Servidio, S., Valentini, F., Vásconez, C.L., Yang, Y., Malara, F., Matthaeus, W.H. & Veltri, P. 2017 Colliding Alfvénic wave packets in magnetohydrodynamics, Hall and kinetic simulations, Revisiting a classic: the Parker-Moffatt problem. *Journal of Plasma Physics* **83**, 905830105.

For Peer Review

Pezzi, O. 2017 Solar wind collisional heating. *Journal of Plasma Physics* **83**, 555830301.

Pezzi, O., Servidio, S., Perrone, D., Valentini, F., Sorriso-Valvo, L., Greco, A., Matthaeus, W.H. and Veltri, P. 2018 Velocity-Space Cascade in Magnetized Plasmas: Numerical Simulations. Submitted to *Physics of Plasmas*. arXiv:1803.01633

Politano, H. & Pouquet, A. 1998 Dynamical length scales for turbulent magnetized flows. *Geophysical Research Letters* **25**, 273.

Pucci, F., Vasconez, C.L., Pezzi, O., Servidio, S., Valentini, F., Matthaeus, W.H., & Malara, F. 2016 From Alfvén waves to kinetic Alfvén waves in an inhomogeneous equilibrium structure. *Journal of Geophysical Research: Space Physics* **121**, 1024–1045.

Retinò, A., Sundkvist, D., Vaivads, A., Mozer, F., André, M. & Owen, C.J. 2007 In situ evidence of magnetic reconnection in turbulent plasma. *Nature Physics* **3**, 235.

Roberts, O.W., Li, X., Alexandrova, O. & Li, B. 2016 Observation of an MHD Alfvén vortex in the slow solar wind. *Journal of Geophysical Research: Space Physics* **121**, 3870.

Schekochihin, A.A., Parker, J.T., Highcock, E.G., Dellar, P.J., Dorland, W. & Hammett, G.W. 2016 Phase mixing versus nonlinear advection in drift-kinetic plasma turbulence. *Journal of Plasma Physics* **82**, 905820212.

Scudder, J. & Daughton, W. 2008 "Illuminating" electron diffusion regions of collisionless magnetic reconnection using electron agyrotropy. *Journal of Geophysical Research* **113**, A06222.

Schwartz, S.J., Hellinger, P., Bale, S.D., Owen, C., Nakamura, R., Vaivads, A., Sorriso-Valvo, L., Liu, W., Wimmer-Schweingruber, R., Fujimoto, M., & Mann, I. 2011 Special Issue: Cross-Scale Coupling in Plasmas Preface. *Planetary and Space Sciences* **59**, 447.

Servidio, S., Matthaeus, W. H., & Dmitruk, P. 2008 Depression of nonlinearity in decaying isotropic MHD turbulence. *Physical Review Letters* **100**, 095005.

Servidio, S., Valentini, F., Califano, F. & Veltri, P. 2012 Local kinetic effects in two-dimensional plasma turbulence. *Physical Review Letters* **108**, 045001.

Servidio, S., Osman, K.T., Valentini, F., Perrone, D., Califano, F. Chapman, S., Matthaeus, W.H. & Veltri, P. 2014 Proton kinetic effects in Vlasov and solar wind turbulence. *The Astrophysical Journal Letters* bf 781, L27.

Servidio, S., Valentini, F., Perrone, D., Greco, A., Califano, F., Matthaeus W.H., & Veltri, P. 2015 A kinetic model of plasma turbulence. *Journal of Plasma Physics* **81**, 328510107.

Servidio, S., Chasapis, A., Matthaeus, W.H., Perrone, D., Valentini, F., Parashar, T.N., Veltri, P., Gershman, D., Russell, C.T., Giles, B., Fuselier, S.A., Phan, T.D. & Burch, J. 2017 Magnetospheric multiscale observation of plasma velocity-space cascade: Hermite representation and theory. *Physical Review Letters* **119**, 205101.

Sorriso-Valvo, L., Carbone, V., Veltri, P., Consolini, G., & Bruno, R. 1999 Intermittency in the solar wind turbulence through probability distribution functions of fluctuations. *Geophysical Research Letters* **26**, 1801.

Sorriso-Valvo, L., Carbone, V., Noullez, A., Politano, H., Pouquet, A. & Veltri, P. 2002 Analysis of cancellation in two-dimensional magnetohydrodynamic turbulence. *Physics of Plasmas* **9**, 89.

Sorriso-Valvo, L., Marino, R., Carbone, V., Noullez, A., Lepreti, F., Veltri, P., Bruno, R., Bavassano, B. & Pietropaolo, E. 2007 Observation of inertial energy cascade in interplanetary space plasma. *Physical Review Letters* **99**, 115001.

Sorriso-Valvo, L., Marino, R., Lijoi, L., Perri, S. & Carbone, V. 2015 Self-consistent castaing distribution of solar wind turbulent fluctuations. *The Astrophysical Journal* **807**, 86.

Sorriso-Valvo, L., Carbone, F., Perri, S., Greco, A., Marino, R. & Bruno, R. 2018 On the statistical properties of turbulent energy transfer rate in the inner heliosphere. *Solar Physics* **293**, 10.

Swisdak, M. 2016 Quantifying gyrotropy in magnetic reconnection. *Geophysical Research Letters* **43**, 43.

Tessein, J.A., Matthaeus, W.H., Wan, M., Osman, K.T., Ruffolo, D. & Giacalone, J. 2013 Association of suprathermal particles with coherent structures and shocks. *The Astrophysical Journal Letters* **776**, L8.

For Peer Review

Vaivads, A., Retinó, A., Soucek, J., Khotyaintsev, Yu.V., Valentini, F., Escoubet, C.P. *et al.* 2016 Turbulence Heating ObserveR - satellite mission proposal. *Journal of Plasma Physics* **82**, 905820501.

Valentini, F., Travnicek, P., Califano, F., Hellinger, P. & Mangeney, A. 2007 A hybrid-Vlasov model based on the current advance method for the simulation of collisionless magnetized plasma. *Journal of Computational Physics* **225**, 753.

Valentini, F., Veltri, P., Califano, F. & Mangeney, A. 2008 Cross-scale effects in solar-wind turbulence. *Physical Review Letters* **101**, 025006.

Valentini, F. & Veltri, P. 2009 Electrostatic short-scale termination of solar-wind turbulence. *Physical Review Letters* **102**, 225001.

Valentini, F., Califano, F. & Veltri, P. 2010 Two-dimensional kinetic turbulence in the solar wind. *Physical Review Letters* **104**, 205002.

Valentini, F., Califano, F., Perrone, D., Pegoraro, F. & Veltri, P. 2011 New ion-wave path in the energy cascade. *Physical Review Letters* **106**, 165002.

Valentini, F., Perrone, D. & Veltri, P. 2011 Short-wavelength electrostatic fluctuations in the solar wind. *The Astrophysical Journal* **739**, 54.

Valentini, F., Servidio, S., Perrone, D., Califano, F., Matthaeus, W.H. & Veltri, P.. 2014 Hybrid Vlasov-Maxwell simulations of two-dimensional turbulence in plasmas. *Physics of Plasmas* **21**, 082307.

Valentini, F., Perrone, D., Stabile, S., Pezzi, O., Servidio, S., De Marco, R., Marcucci, F., Bruno, R., Lavraud, B., De Keyser, J., Consolini, G., Brienza, D., Sorriso-Valvo, L., Retinò, A., Vaivads, A., Salatti, M. & Veltri, P. 2016 Differential kinetic dynamics and heating of ions in the turbulent solar wind. *New Journal of Physics* **18**, 125001.

Valentini, F., Vasconez, C.L., Pezzi, O., Servidio, S., Malara, F., & Pucci, F. 2017 Transition to kinetic turbulence at proton scales driven by large-amplitude kinetic Alfvén fluctuations. *Astronomy & Astrophysics* **599**, A8.

Vasconez, C.L., Pucci, F., Valentini, F., Servidio, S., Matthaeus, W.H., & Malara, F. 2015 Kinetic Alfvén wave generation by large-scale phase mixing. *The Astrophysical Journal* **815**, 7.

Wan, M., Matthaeus, W.H., Roytershteyn, V., Karimabadi, H., Parashar, T., Wu, P., & Shay, M. 2015 Intermittent Dissipation and Heating in 3D Kinetic Plasma Turbulence. *Physical Review Letters* **114**, 175002.

Yang, Y., Matthaeus, W.H., Parashar, T., Wu, P., Wan, M., Shi, Y., Chen, S., Roytershteyn, V., & Daughton, W. 2015 Intermittent Dissipation and Heating in 3D Kinetic Plasma Turbulence. *Physics Review E* **95**, 061201(R).

For Peer Review